Hindawi Publishing Corporation
International Journal of Rotating Machinery
Volume 2015, Article ID 679576, 13 pages
http://dx.doi.org/10.1155/2015/679576

Research Article

Flow Modeling in Pelton Turbines by an Accurate Eulerian and a Fast Lagrangian Evaluation Method

A. Panagiotopoulos,[1,2] A. Židonis,[1] G. A. Aggidis,[1] J. S. Anagnostopoulos,[2] and D. E. Papantonis[2]

[1]*Lancaster University Renewable Energy Group and Fluid Machinery Group, Engineering Department, Engineering Building, Bailrigg, Lancaster, Lancashire LA1 4YW, UK*
[2]*School of Mechanical Engineering, Laboratory of Hydraulic Turbomachines, National Technical University of Athens, 9 Heroon Polytechniou, Zografou, 15780 Athens, Greece*

Correspondence should be addressed to G. A. Aggidis; g.aggidis@lancaster.ac.uk

Received 26 June 2015; Accepted 21 October 2015

Academic Editor: Robert C. Hendricks

The recent development of CFD has allowed the flow modeling in impulse hydro turbines that includes complex phenomena like free surface flow, multifluid interaction, and unsteady, time dependent flow. Some commercial and open-source CFD codes, which implement Eulerian methods, have been validated against experimental results showing satisfactory accuracy. Nevertheless, further improvement of accuracy is still a challenge, while the computational cost is very high and unaffordable for multiparametric design optimization of the turbine's runner. In the present work a CFD Eulerian approach is applied at first, in order to simulate the flow in the runner of a Pelton turbine model installed at the laboratory. Then, a particulate method, the Fast Lagrangian Simulation (FLS), is used for the same case, which is much faster and hence potentially suitable for numerical design optimization, providing that it can achieve adequate accuracy. The results of both methods for various turbine operation conditions, as also for modified runner and bucket designs, are presented and discussed in the paper. In all examined cases the FLS method shows very good accuracy in predicting the hydraulic efficiency of the runner, although the computed flow evolution and the torque curve exhibit some systematic differences from the Eulerian results.

1. Introduction

The design of Pelton and other impulse type turbines was based on existing know-how, and any design improvements were mainly conducted after extensive experimental testing by the trial-and-error method. In recent years significant effort has been directed towards a better understating of the details of the complex unsteady flow in the runner, with the aid of Computational Fluid Dynamics (CFD) and modern numerical modeling [1]. Commercial software has been developed and used based on Eulerian mesh-type codes like Ansys-CFX [2, 3] and Ansys-Fluent [4, 5] that are designed to simulate the flow in various physical problems. Also, a number of noncommercial software tools have been developed like the Open FOAM [6], as also various Lagrangian approaches, like the Smoothed Particle Hydrodynamics method [7] or other in-house codes like the Fast Lagrangian Simulation (FLS) [8, 9] that were developed to solve specific flow problems.

At first, the Eulerian mesh-type methods were used in order to simulate the flow in Pelton turbines. Several papers have been published investigating the flow in the injector [10–12], in the stationary buckets [4], and in the rotating runner [2, 5], as well as analyzing specific flow mechanisms like cavitation [13].

In most cases, commercial CFD software was used as it can simulate the flow with adequate accuracy, in order to calculate the hydraulic efficiency and evaluate the geometrical characteristics of the turbine. Nevertheless, the computational cost is too high to be used for multiparametric design optimization, where thousands of flow evaluations are required to obtain an optimum design solution. Other

meshless simulation methods based on the Lagrangian approach have also been developed. The most popular one is the Smooth Particle Hydrodynamics (SPH) methodology [14, 15], the computational cost of which is, however, comparable to the Eulerian methods, while further development and validation are needed to improve its accuracy.

In order to reduce the computational cost, a particulate method based on the Lagrangian approach has been developed by the Laboratory of Hydraulic Turbomachines, NTUA [8, 9]. This Fast Lagrangian Simulation (FLS) method introduces appropriate adjustable terms in the flow particle equations to approximate the various viscous and pressure effects of their trajectories.

The aim of the present paper is to evaluate the performance and accuracy of the FLS method by comparing the results against the corresponding ones of the Ansys-Fluent commercial software [16, 17] that uses the Volume-of-Fluid (VOF) technique to simulate the jet and free surface flow in the runner. The accuracy of the latter has been validated against experimental results in Pelton runners [18–21].

In the present study, the appropriate computational domain, mesh density, and settings of the VOF technique are at first investigated to achieve the best compromise of accuracy and computational cost. Then, an initial test case is defined including the exact geometrical characteristics of a Pelton model runner installed in the laboratory. The FLS and Fluent software are applied to various operating condition cases of this turbine, and for runners of different design, in order to compare their numerical performance based on the time history of torque development and on the hydraulic efficiency of the runner.

2. Numerical Modeling of the Flow

Two computer codes were used for the simulation of the complex flow in a rotating Pelton runner, the commercial software Fluent and the in-house software FLS. The Fluent code [16] is capable of solving multiphase flow problems with free surfaces, which are highly relevant to impulse turbines. It is based on the spatial discretization of the Reynolds Averaged Navier-Stokes equations on a computational mesh using cell-centered numerics (finite volumes) and offers flexibility in choosing between segregated based and coupled based solver.

The two-fluid-flow (air and water) problem with free surface, like the Pelton runner case, is being solved using the established Volume-of-Fluid (VOF) method. VOF is an Eulerian-Eulerian method based on tracking and locating the fluid-fluid interface. An additional factor, the volume fraction, is introduced which represents the percentage of each fluid volume in every cell. The method can model two or more immiscible fluids by solving a single set of momentum equations and tracking the volume fraction of each of the fluids throughout the domain.

For the two-phase (water-air) flow in Pelton runners the air is defined as the primary phase and the water as secondary, so as the tracking of the interface between them is accomplished by the solution of a continuity equation for the volume fraction of the secondary phase that has the following form:

$$\frac{1}{\rho_q}\left[\frac{\partial}{\partial t}\left(a_q\rho_q\right)+\nabla\cdot\left(a_q\rho_q\vec{v}_q\right)\right]=\sum_{p=1}^{n}\left(\dot{m}_{pq}-\dot{m}_{qp}\right), \quad (1)$$

where $\dot{m}_{pq}$ is the mass transfer from phase p to phase q and $\dot{m}_{qp}$ the opposite and a_q is the volume fraction and ρ the density. The present application of Fluent-VOF software for flow simulation in Pelton runners is analyzed in Section 4.

2.1. Fast Lagrangian Simulation Method. The Fast Lagrangian Simulation (FLS) [8, 9] is a single-phase flow simulation method, and it is based on the tracking of a representative number of fluid particles in order to model and calculate the flow pattern and the energy exchange in the rotating runner of impulse hydro turbines. The exact water-air interface pattern is not required for such computations, though the flow width on the bucket surface could be estimated from the properties of the tracked particles.

The water jet is being separated into discrete particles, as shown in Figure 1, and their equations of motion are numerically integrated until they exit from the inner bucket surface. The jet is considered ideal, that is, with uniform initial velocity, and the flow frictionless. Also, due to the periodic symmetry conditions only two consecutive buckets were modeled.

The fluid particle equations are solved in a rotating orthogonal system of reference and are expressed in Cartesian coordinates as follows (bucket rim is on the xy level):

$$\begin{aligned}\frac{d^2x}{dt^2}&=f_x(x,y),\\ \frac{d^2y}{dt^2}&=f_y(x,y)+\omega^2y+2\omega\frac{dz}{dt},\\ \frac{d^2z}{dt^2}&=f_z(x,y)+\omega^2z-2\omega\frac{dy}{dt},\end{aligned} \quad (2)$$

where ω is the angular rotation speed of the runner and f_x, f_y, and f_z are the additional terms, functions of the local surface geometrical characteristics.

The particle motion equations do not contain particle interaction or mechanical losses terms and hence they cannot reproduce the real flow picture in the bucket. For this reason, the FLS model introduces a number of additional terms in order to account for the various hydraulic losses (impact, friction, and change direction), as well as for the pressure effects that control the spreading of the surface flow in the bucket, which are activated after the impact of a particle on the bucket surface. More specifically, the friction losses on the bucket surface are modeled as reduction of particle kinetic energy by a factor analogous to the square of particle velocity and to sliding distance; hence the particle velocity magnitude after a time step Δt becomes

$$V_p'\approx V_p\cdot\left(1-C_f\cdot V_p\cdot\Delta t\right). \quad (3)$$

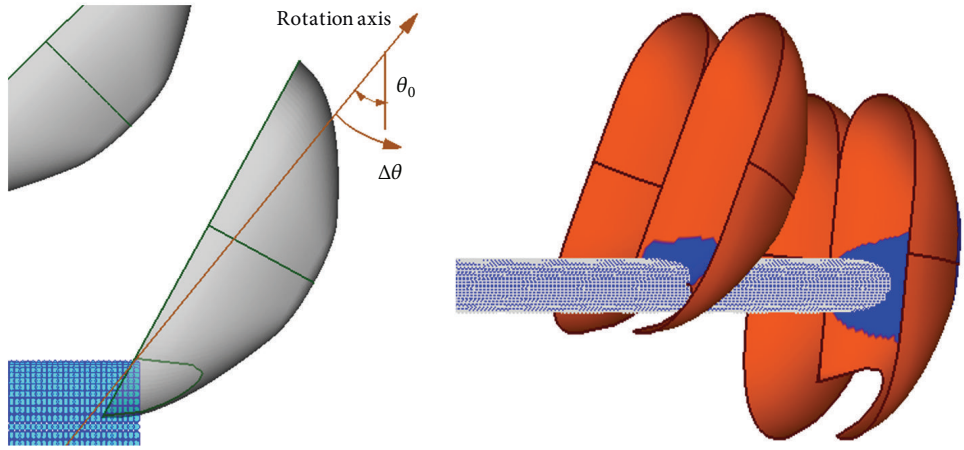

Figure 1: FLS modeling: jet discretization and jet-bucket interaction starting angle (a); surface flow simulation and representation (b).

The energy losses at the jet impact on the bucket are taken analogous to the square of the normal to the surface particle velocity component, and this gives

$$V_p' \approx V_p \cdot \left(1 - C_i \cdot \cos^2 \varphi_i\right), \tag{4}$$

where φ_i is the particle impingement angle.

The progressive change of particle's path direction (and momentum) as it slides along the curved bucket surface also causes minor energy losses, which are modeled using a term similar to the impact losses:

$$V_p' \approx V_p \cdot \left(1 - C_p \cdot \cos^2 \Delta\varphi\right), \tag{5}$$

where $\Delta\varphi$ is the angular change in direction of the sliding particle during the time step Δt.

The adjustable coefficients C_f, C_i, and C_p are introduced in the above modelling equations (3)–(5) so as they can be tuned in order to match the results with the corresponding ones obtained by more accurate CFD methods or by experimental studies. This constitutes an important feature of the FLS model that can significantly improve the reliability and accuracy of its results, at almost no additional computer cost.

Finally, in order to model the pressure effects on the surface flow spreading and evolution, a particle acquires at the impact point an artificial "spreading" velocity component perpendicular to its impacting plane ($\vec{V}_S$, Figure 2), while its main velocity component is correspondingly reduced to preserve kinetic energy. The magnitude of this spreading velocity depends on the radial and circumferential position of a particle in the jet cross section, and it is determined by two corresponding additional adjustable coefficients [8].

The first tuning of the above coefficients has been carried out with the aid of available experimental data in a Pelton turbine model, so as to minimize the squared differences between the measured and the computed characteristic curves of turbine efficiency [8]. This problem was solved with an optimization software based on evolutionary algorithms, considering these coefficients as free variables, the values of

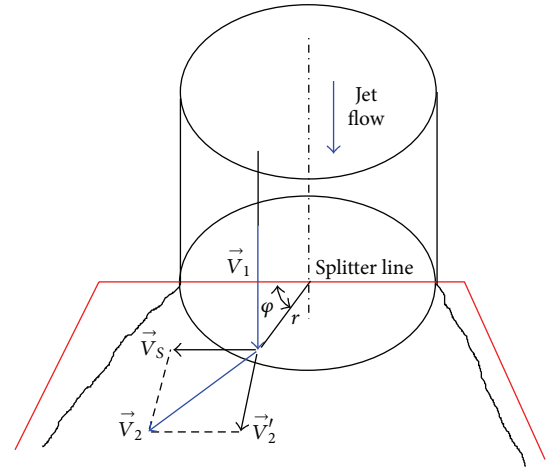

Figure 2: Sketch of surface flow spreading modeling.

which are iteratively optimized from generation to generation.

It must be noted that some secondary flow mechanisms developed during the jet-runner interaction, like the jet cut or the attached flow at the back face of the bucket, are not modeled by the FLS method. However, their effect on the energy transfer and hydraulic efficiency of the runner are taken into account in an implicit manner through the above adjustable terms. More details on the model formulation and its regulation procedure, as well as on the parametric design of the runner, can be found in [8].

The application of the FLS model for the simulation of the jet-runner interaction in Pelton turbines requires only a mathematical/numerical description of the inner bucket surface, and since it does not use a computational mesh, it can be very easily adapted to any design or operation data of the runner. Also, a specific postprocessing algorithm is developed and used for the presentation and comparison of FLS results (e.g., Figure 1).

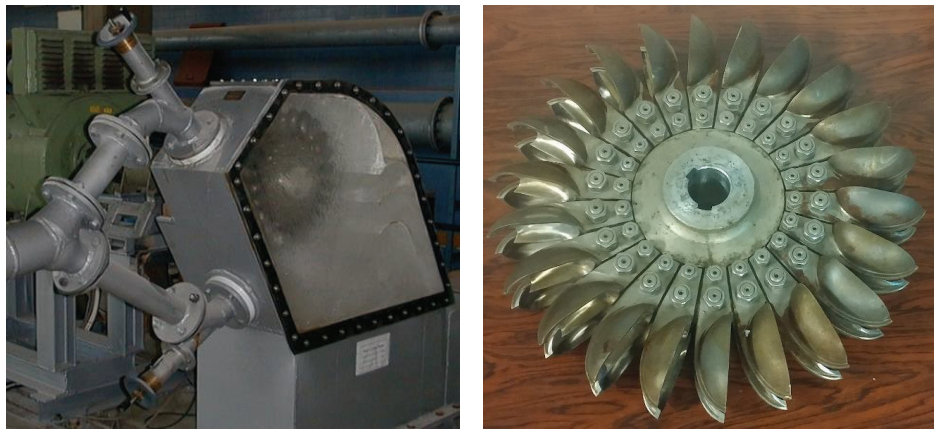

Figure 3: Pelton model turbine and its runner installed at the LHT.

3. Test Case

The geometrical characteristics of the Pelton model turbine used as a reference case correspond to a Pelton turbine installed in the LHT, at the National Technical University of Athens (Figure 3) [22]. The pitch diameter of the runner is 400 mm, and the axis is horizontal with two injectors of 36 mm nozzle diameter. The net head, the rotational speed, and the nozzle stroke can be adjusted for experimental reasons according to the IEC standards [23]. The runner contains 22 buckets which were designed and constructed in the lab, based on old literature guidelines [24], as shown in Figure 4. Therefore the achieved efficiency of the turbine is smaller than that suggested in more recent bibliography [25], which refers to the state-of-the-art turbines. Nevertheless, all geometrical characteristics of modern runners and buckets are included, and hence the flow mechanisms that take place during the interaction of the free jet with the runner are the same.

Although the Pelton turbine is installed at the laboratory test rig and the total efficiency of the turbine has been measured experimentally, a direct comparison between numerical and experimental results is not easy. The measured efficiency represents the total efficiency of the turbine including all losses according to the IEC standards [23], while only the hydraulic efficiency of the runner can be calculated numerically. So, the comparison would require the estimation of minor losses like the losses in the nozzle, the mechanical losses, and the windage losses caused by the movement of the runner and its interaction with the misty environment into the casing. These losses highly depended on the quality of the turbine construction, the geometrical characteristics of the casing, and the type of the bearings. So, their estimation would introduce considerable uncertainty to an experimentally derived efficiency of the runner. For this reason, the present work focuses on the comparison and evaluation of the performance and accuracy of the two software tools, when used for Pelton turbines analysis and design. The provided detailed geometric data of the runner (Figure 4) can be used as benchmark for the validation and evaluation of other numerical modelling tools and methods.

The comparison of FLS and Fluent results was initially performed for the reference operating conditions of the Pelton turbine: one injector is operating with nozzle stroke 12 mm, which corresponds to the best efficient point (BEP) of the runner with one injector, according to the experimental results. The rotation speed was 1000 rpm, the diameter of the jet was 12 mm, and its axial velocity was uniform and equal to 44.45 m/s. For modeling purposes, the velocity profile of the jet is taken uniformly.

4. Accurate Eulerian Flow Evaluation

The basic steps for the numerical simulation with a mesh-type Eulerian method of Fluent software are the design of the appropriate 3D geometry, the construction of the grid covering the whole domain, and the solution of the system of flow equations. The simulated geometry is designed using the SolidWorks 12 commercial software, and it was essential to avoid very small edges and narrow faces or volumes. The geometry was separated into two domains, the rotating domain, which contains the buckets, and the stationary domain from where the free jet is injected. Due to the heavy computing requirements and thanks to the periodic symmetry of the runner, only two consecutive buckets were modeled (Figure 5). Also, only the half symmetric part of the domain was considered, a common practice in modeling Pelton turbines.

4.1. Torque and Efficiency Calculation. The hydrodynamic torque and the hydraulic efficiency of the runner are computed after completing the evaluation of a jet-bucket interaction flow, starting from the moment of impingement until the evacuation of the bucket.

During the unsteady flow simulation the total torque on a bucket is calculated at every time step (or its tangential position φ) by adding the torque on the inner surface of the first bucket to the torque on the backside of the second bucket, as shown in Figure 5. The latter is developed due to the adherence of a jet portion after it is cut by the bucket (Coanda effect), and also due to possible interference between

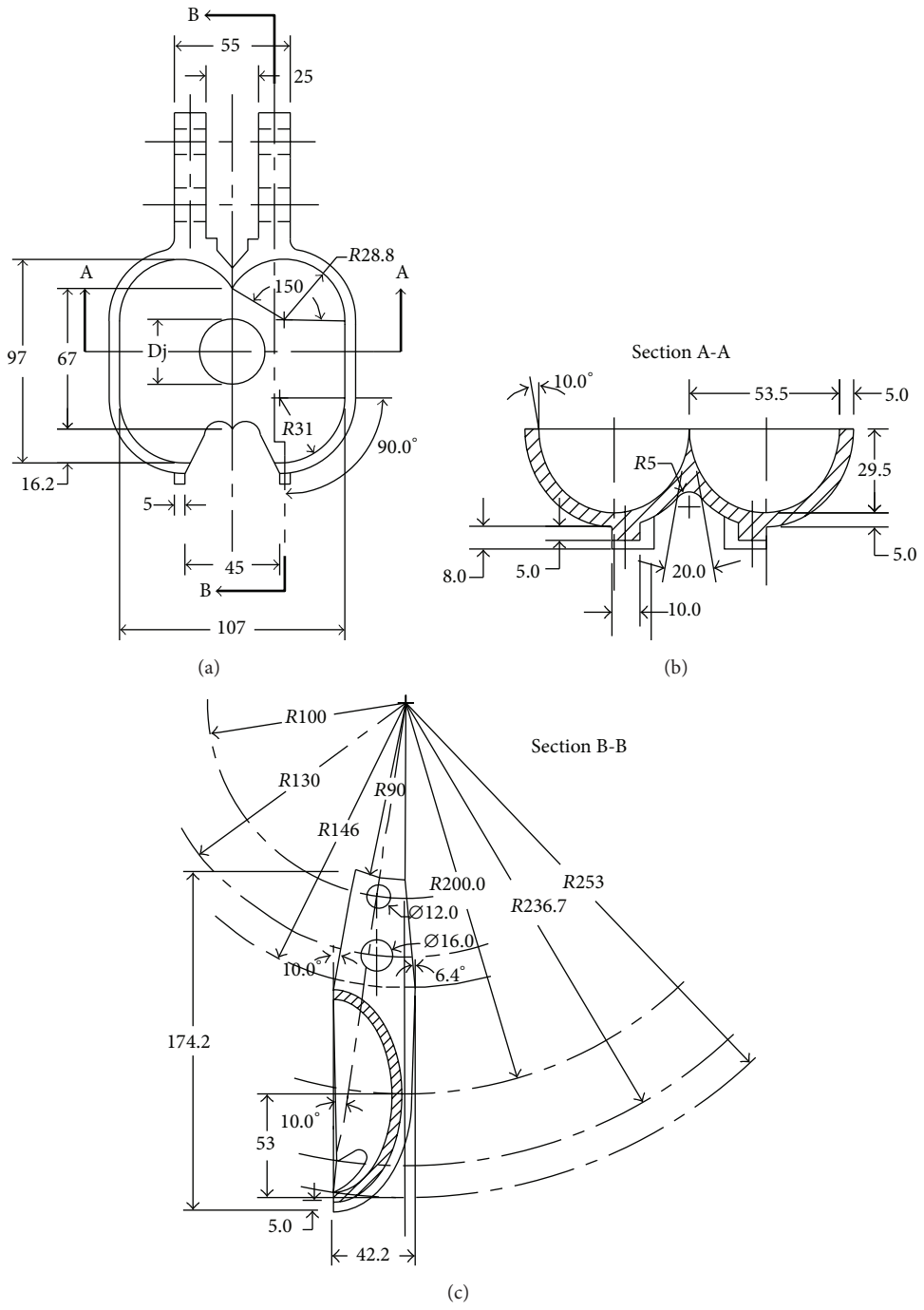

Figure 4: Details of the runner design [22].

the back surface of the bucket and the outflow water from the first bucket

$$T_r(\varphi) = T_{\text{in}}(\varphi) + T_b\left(\varphi + \frac{360}{N_b}\right), \tag{6}$$

where T_r is the torque in a single bucket, T_{in} and T_b are the torque at the inner and backside surfaces, respectively, and N_b is the number of buckets on the runner (22 for this case).

The torque curve of one bucket against the rotating angle is repeated periodically every $360^\circ/N_b$, where N_b is the total number of buckets (22 in this case). The sum of the torque values of all curves for every angular position represents the torque curve of the runner. So the total mechanical energy transferred to the shaft during one rotation can be calculated from the equation:

$$W = \int_0^{360} T(\varphi)\, d\varphi, \tag{7}$$

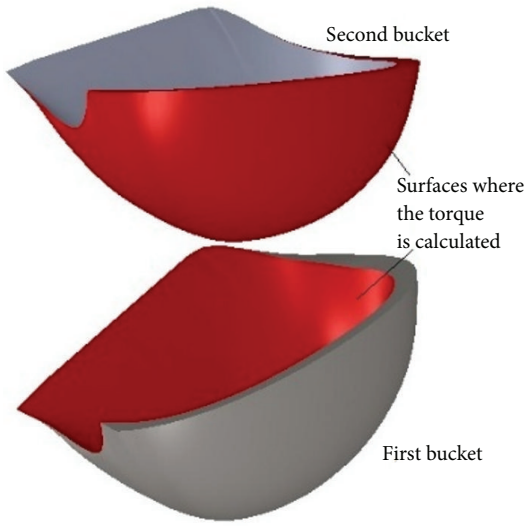

Figure 5: Two consecutive half buckets used to calculate the total runner torque.

where $T(\varphi)$ is the torque on a single bucket and φ the angular position of the runner ($\varphi = \omega \cdot \Delta t$, Δt is the time step and ω is the angular speed).

The runner power is then calculated as

$$P = \frac{W \cdot \omega}{360} \tag{8}$$

while the power of the water jet is

$$P_w = \frac{\pi\rho}{8} D_{\text{jet}}^2 u_{\text{jet}}^3, \tag{9}$$

where ρ is the water density and u_{jet}, D_{jet} are the velocity and diameter of the jet.

Finally, the hydraulic efficiency of the runner is defined as

$$\eta = \frac{P}{P_w}. \tag{10}$$

4.2. Computational Grid and Accuracy of Results. The computational grid was made using the Ansys Workbench commercial software package after an extensive investigation due to its strong influence on the final speed of the simulation and the accuracy of the results. The elements around the rotating buckets and the cylindrical jet were tetrahedral and hexahedral, respectively, as shown in Figure 6. In addition, an inflation layer was adjusted at the inner and backside faces of the buckets in order to reduce the $y+$ value below 50 when the k-ω turbulence model is used. The inflation consists of 5 layers of hexahedral cells with very small thickness placed at the region where the boundary layer is being developed.

The quality of the mesh is acceptable as the minimum orthogonal quality is 0.15 while the average is 0.87. Since the position of the jet changes transiently it is not possible to refine the shear layer; therefore the entire mesh had to be fine enough to have minimum impact on the simulated efficiency. In addition, as the unstructured tetrahedral mesh type can decrease the accuracy of the results, a very dense mesh was used at the area of high importance. The minimum and maximum cell volume are 1.1×10^{-12} m^3 and 1.5×10^{-8} m^3, respectively.

Moreover, a study about the appropriate mesh size was carried out in order to achieve independency between the size of the mesh and the accuracy of the results. The same case with the same settings was simulated for four different sizes of tetrahedral mesh. The densest mesh consists of about 5.16 million elements and it was found that the maximum possible accuracy in terms of the calculated efficiency was achieved. The efficiency dependence on the mesh density is represented in Figure 7.

From the above results it can be deduced that the independency was achieved for meshes with more than 2.4 M cells. For the present simulations, a mesh with approximately 2.8 M cells was adopted to ensure the accuracy of the results. The simulations were carried out using a four-core Intel Xeon, 3.4 GHz, and 16 GB RAM. The CPU-time was almost proportional to the size of the mesh and for the 2.4 M cells it is about 3.2 days.

The torque variation curves on a bucket obtained using different density meshes are presented in Figure 8, where the angular position of the bucket is taken zero at its vertical or normal to the jet position (Figure 1). At the start of jet-runner interaction (-40°) a negative torque can be observed caused by the interaction of the jet with the back surface of the bucket. At this stage the jet is starting entering the bucket moving almost in parallel with the back surface, thus causing there a high pressure region, as shown in Figure 9, responsible for the negative torque. Just afterwards, the torque is increasing as more water interacts with the inner surface. At an angle of about -22 degrees the second bucket begins to interact with the jet, leaving less water to move towards the first bucket. This reduced amount of water that moves towards the first bucket is not smooth due to divergence of the jet caused by Coanda effect (Figure 10). This diverged portion of water hits the first bucket at around -10 degrees, causing an irregular increment of the torque (Figure 8). After this point, the developed torque decreases smoothly as the water is leaving the bucket, until evacuation completes at $+30$ degrees. The total jet-runner interaction period lasts about 70° rotational angle of the runner.

4.3. Turbulence Modeling and Computational Details. During the simulations using Fluent many different settings were tested, some of which had strong influence on the results. The 3D single precision solver was selected in order to reduce the computational cost as no important difference was observed compared to double precision simulation. The appropriate model for the simulation is the *Volume-of-Fluid* (VOF), with pressure-velocity coupling solution method. The pressure-based *coupled* scheme increases the computation time but provides a much more stable and reliable solution compared to the *SIMPLE* or *PISO* schemes. The transient flow is simulated both as inviscid and as turbulent using the k-ω SST model, in order to assess the impact of the friction and turbulent losses on the efficiency. The time step was constant and equal to 5 μs, which corresponds to 0.03 degrees

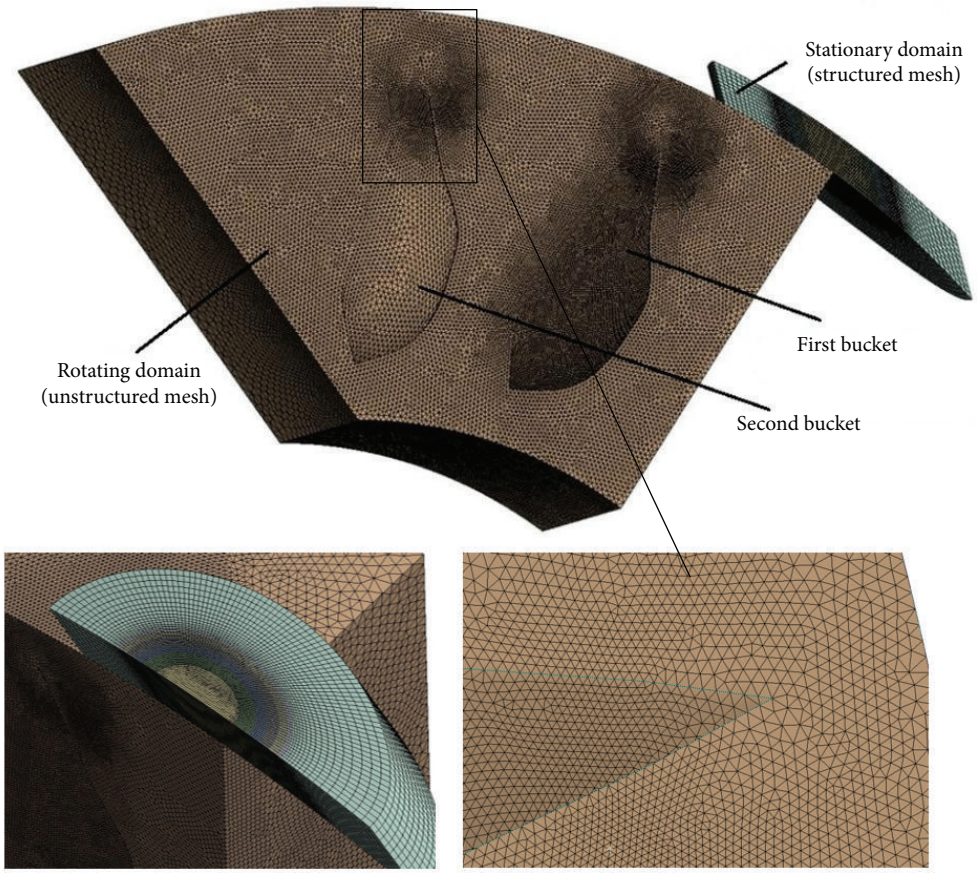

Figure 6: Computational domain and structure of the 3D mesh.

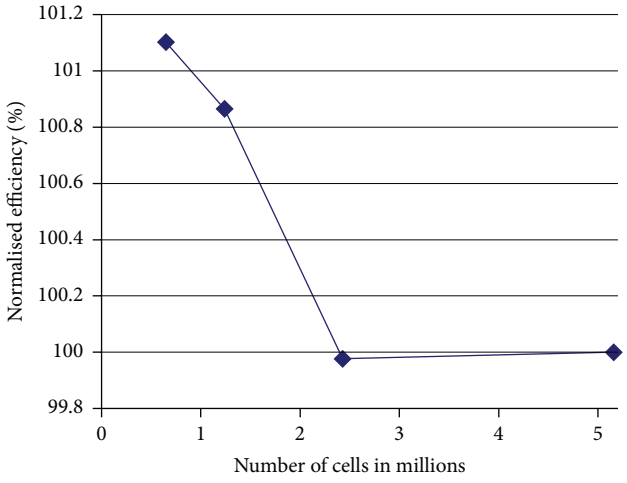

Figure 7: Runner efficiency response to mesh refinement.

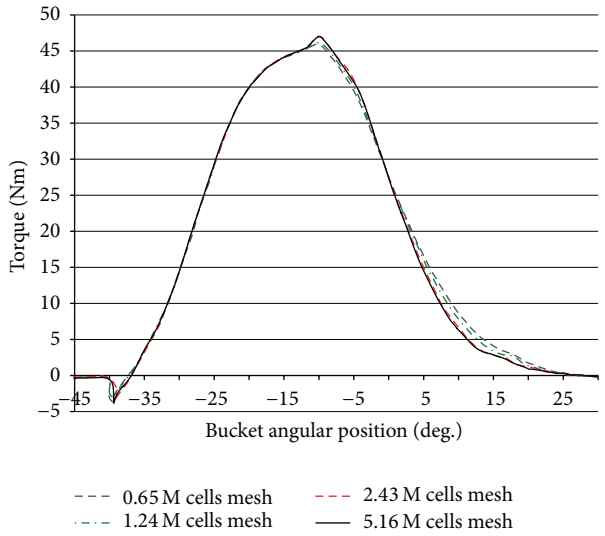

Figure 8: Individual torque curves of mesh refinement simulations.

of runner rotation angle, while the maximum number of iterations was set to 10, as suggested in the literature [17]. The solution was not influenced by the time step as soon as the continuity residuals were under 10^{-3} even if most of the time during simulation they were close to 10^{-4}, where the residuals target was set. The continuity residuals target for convergence was set to 10^{-4}, while the rest residuals were always below 10^{-5}.

The highest flow velocities in the computed field correspond to the free jet velocity, which is about 45 m/s. In addition, the coupled implicit scheme was used, and therefore

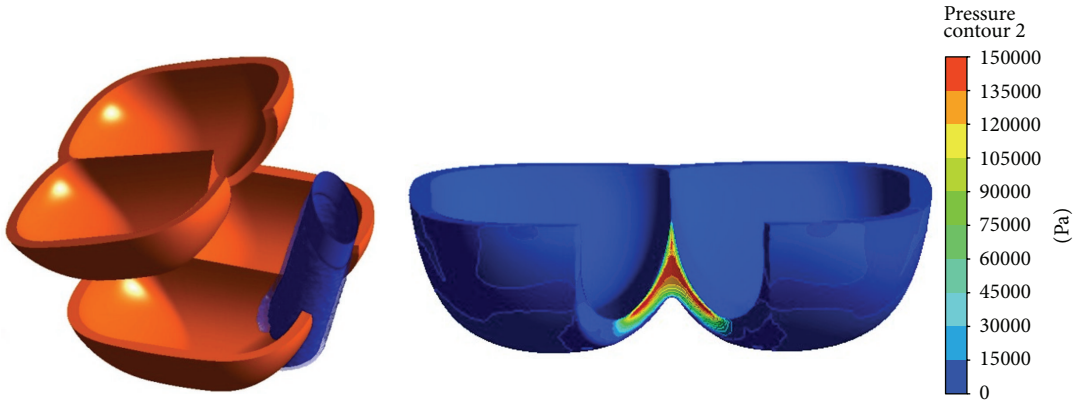

Figure 9: High pressure development at the backside while the jet is entering the bucket.

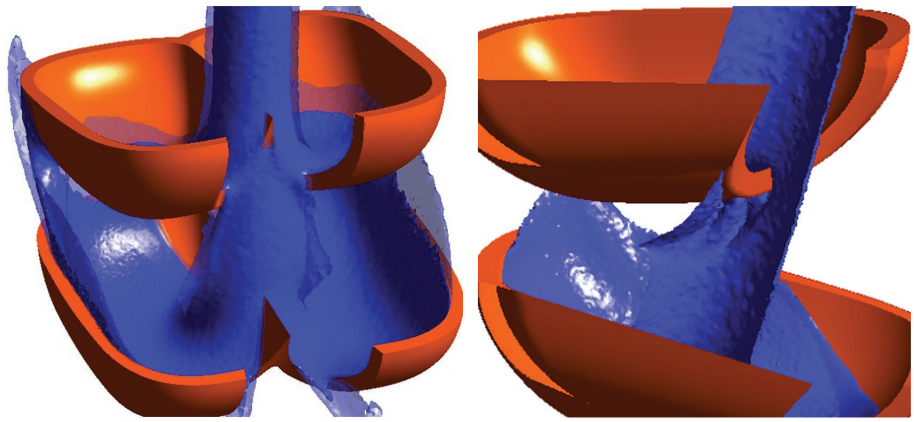

Figure 10: Diverged flow moving towards the first bucket.

the Courant number had a minor effect since the point Gauss-Seidel scheme used is unconditionally stable, according to the linear stability theory. Consequently, the default value of 200 was used while different values have negligible influence in the solution.

Finally, the possible effect of surface tension was considered by using the "continuum surface force" model, which is available in Fluent platform. However, and in agreement with the literature [2], the implementation of this model has negligible effect on the simulated flow in a Pelton runner. Moreover, the Weber number of the relatively high velocity flow in the bucket is large (>50), and only at the last evacuation stage, where the remaining water forms very thin and separated films on the bucket surface, the Weber number may be considerably reduced. But the contribution of this stage to the energy exchange and the developed torque is minor. Consequently, the surface tension effects are ignored in the simulations.

A comparison between the torque curves calculated with inviscid and k-ω SST turbulence model is shown in Figure 11. As can be observed in this figure, the developed torque is slightly lower for the turbulent flow simulation, while the corresponding efficiency is about 3.5% reduced (84.8% compared to 88.3% of the inviscid flow). This is mainly due to the friction losses at the flow boundary layer along the inner bucket surface, and the impact losses of the entering jet flow.

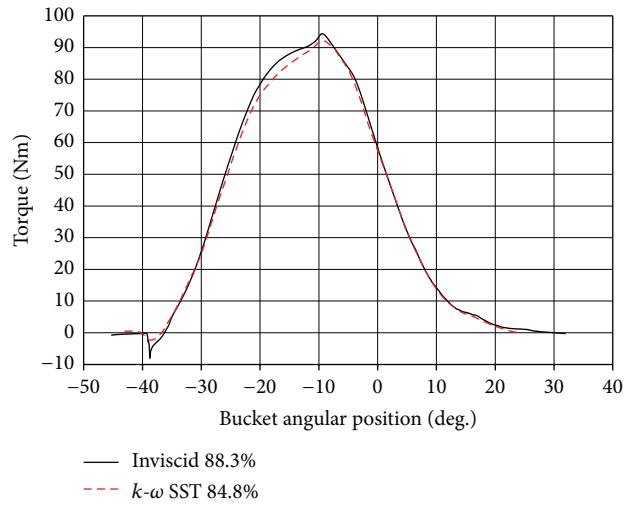

Figure 11: Comparison of inviscid and turbulent flow numerical results.

5. FLS Method Application and Comparison with VOF

Tracking of about 5000 fluid particle trajectories using a time step for integration of 2×10^{-5} sec was found to produce statistically accurate results for all cases examined in the present study. A complete flow evaluation requires about 10 CPU sec in a modern PC, which is almost 4 orders of magnitude less than the corresponding evaluation time using Fluent. This significant advantage of the FLS method allows its application for multiparametric design optimization studies of impulse turbine runners, in conjunction with modern optimization software.

After completion of the fluid particles tracking, the FLS postprocessing algorithm computes the runner performance in terms of the developed torque on the blades and the hydraulic efficiency of the runner, while it can also calculate the local forces exerted on the blade during the energy conversion procedure. The mechanical energy transferred to each bucket is obtained from the equation of conservation of angular momentum [8]:

$$W = \rho Q_u \left(R_{\text{run}} u_{\text{jet}} - \frac{1}{N} \sum_i r_i w_i \right), \tag{11}$$

where Q_u is the cumulative flow that enters each bucket, R_{run} is the runner pitch radius, and w_i is the tangential velocity component of particle i at the moment it exits the bucket at radial distance r_i. N is the total number of fluid particles that interact with a single bucket. The hydraulic efficiency of the runner can then be obtained as the ratio of the developed mechanical power divided by the corresponding net hydraulic power at the inlet, as in (10).

The performance and accuracy of the FLS method are evaluated by comparing its results with the corresponding ones of Fluent software, for a number of different cases. The comparison is based on the computed values of the runner hydraulic efficiency, the pattern of the torque curve, and the distribution of the surface flow on the inner bucket face. At first, the comparison is carried out for the design point of the laboratory model turbine, for which the coefficients of the FLS model are calibrated.

Next, two cases with different flow rates, one lower and one higher, were simulated maintaining the remaining parameters constant. An additional simulation took place for different head and rotating speed of the turbine that corresponds to a smaller specific speed of the runner. Also, in another test case the geometry of the runner was changed by reducing the number of buckets from 22 to 18. Finally, a comparison is made for another Pelton runner with different bucket design.

5.1. Comparison at the Reference Test Point. Firstly, the computational results of the reference test point (BEP) using FLS and Fluent are being compared with each other. In Figure 12 the resulted total torque in one bucket is compared. It can be observed that the agreement between the curves is good, as the general shape and the maximum torque are the same. The small differences can be explained due to the inability

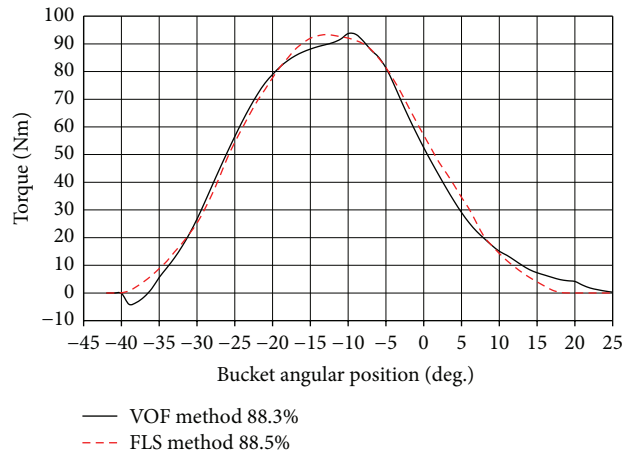

Figure 12: Comparison of the computational results for the reference point.

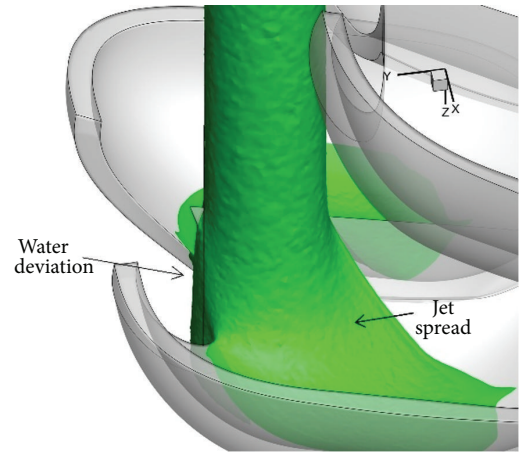

Figure 13: Water deviation close to the solid surface calculated with Fluent.

of the FLS method to model secondary mechanisms, like the previously mentioned negative torque at the beginning of the interaction with the jet, and the Coanda effect, thus resulting in a smoother torque curve. Another minor phenomenon is a small radial deviation of the jet caused when it is cut at the bucket tip, as shown in Figure 13. The amount of deviated water hits the next bucket at a slightly different time (earlier), and this may explain the slightly higher torque values of the VOF in the increasing part of curve of Figure 12.

In addition to the torque results, the spreading rate of the surface flow on the inner bucket surface is also considered in order to adjust the spreading model coefficients of the FLS method. In Figure 14 an isosurface is being represented with green color as it is calculated by Fluent, whereas the black lines are the orbits of the particles obtained by FLS. It can be observed that the surface flow pattern on the solid surface calculated from Fluent and FLS is quite similar, but the spreading rate shows certain differences. After an analysis of the particles' orbits and the velocity fields obtained by the two methods it was ascertained that two main reasons cause this difference.

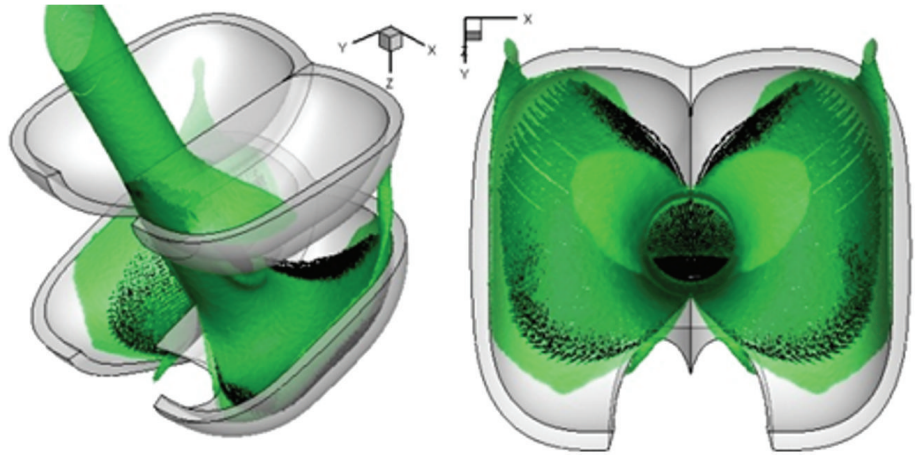

Figure 14: Water phase comparison of FLS (black lines) and Fluent (green areas) simulations.

Firstly, the jet flow as computed by VOF exhibits a significant spread just before it reaches the bucket (Figure 13), due to the high pressure field developed in the impact area below. Consequently, the flow path lines follow a smooth curved orbit before reaching the bucket surface, with the curvature radius being analogous to the radial position with respect to the jet axis. On the other hand, all flow particles of the FLS method move straight until they hit the inner bucket surface and then change direction instantly to flow parallel to the bucket surface. Therefore, during the first interaction stages a flow particle modeled by FLS travels a longer distance to reach to a particular position on the surface than the corresponding one simulated by Fluent. Moreover, the small impact losses of the flow are accounted for at the impact point thus reducing the particles' velocity when they hit the bucket, whereas this is taking place more progressively with Fluent simulation.

For the above reasons, the spreading rate of the surface flow is computed lower of the FLS at the first jet-runner interaction stages, while the outflow as it is being calculated from Fluent starts earlier (Figure 14). To compensate for this difference, the variation limits of the coefficients of the spreading model are properly regulated, by using proper constraints during the optimization procedure of the set of FLS coefficients for the reference case, in order to match also as best as possible both the torque variation curve and the hydraulic efficiency. As a result, the subsequent interaction stage becomes faster with the FLS simulation, and the evacuation of the bucket happens a little earlier (about 7° in Figure 12).

In spite of the inability of FLS method to simulate accurately all flow details and mechanisms, the resulting hydraulic efficiency of the runner is almost equal to that of Fluent (88.3% compared to 88.5%, Figure 12). This confirms the capability of the regulated FLS model to reproduce satisfactory main flow characteristics (e.g., torque curve) and also to implicitly take into account the effects of all secondary flow mechanisms on the efficiency.

5.2. FLS Performance for Different Turbine Loading. In order to evaluate further the FLS method performance, two test cases at different operating points of the turbine are simulated, by changing the flow rate (loading) of the runner. All other design and operation characteristics remain the same except of the jet diameter, which depends on the nozzle opening (or spear valve stroke) of the injector. The first case is for smaller nozzle stroke which corresponds to 50% of the design point flow, while the second is for higher nozzle stroke and 135% of the design flow. The torque curves and the runner efficiency values computed by VOF and FLS methods are presented in Figure 15.

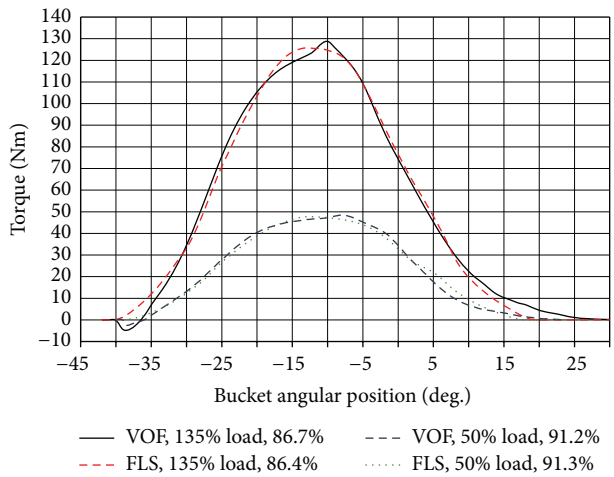

Figure 15: Comparison of VOF and FLS method for off design turbine operation conditions.

The shape of the torque curves shown in this figure is similar to those at the reference point (Figure 12), but the maximum torque is, as expected, analogous to the loading of the runner. The agreement between the FLS and Fluent results is also good in both cases, with the differences of the FLS curves being again at the same regions (nonnegative torque at the beginning, smoother curve, slightly displaced to the right, and faster bucket evacuation).

Moreover, in both cases the calculated efficiency by the FLS method is again very similar to that of the VOF method,

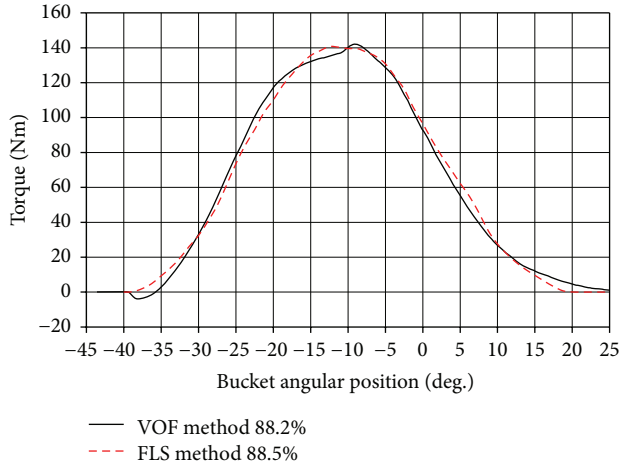

Figure 16: Comparison of VOF and FLS methods for higher hydraulic head.

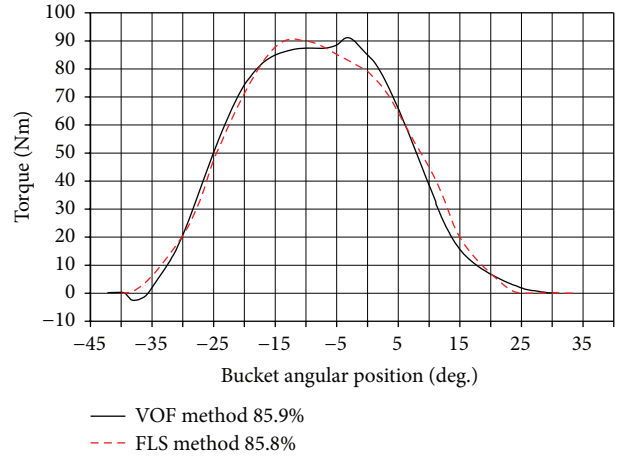

Figure 17: Comparison of VOF and FLS method for different runner design of 18 buckets (from 22).

with the differences being 0.1% and 0.3% (Figure 15), namely, within the order of numerical solution accuracy of Fluent software. It is noted that the increased efficiency of the runner at smaller flow rates is due to the inviscid simulation of the flow, in which the increased friction losses that have a thinner free surface flow along the bucket are not accounted. On the other hand, the obtained reduction of the efficiency higher than the design flow rate is due to a different mechanism: during the evolution of the free surface flow on the bucket surface a portion of water may leave the bucket through the cut edge area, as shown in Figure 14, but not with optimum (minimum) outflow velocity, thus causing a small drop in overall efficiency of the runner. This phenomenon becomes more intense for higher flow rates, due to the wider spread of the surface flow on the bucket.

5.3. FLS Performance for Different Hydraulic Head. In this case, the inlet water pressure was increased by 56% (from 100 m of the reference point), which corresponds to exit jet velocity of 55.7 m/s. The higher jet velocity requires higher rotating speed of the runner, which is calculated equal to 1250 rpm in order to maintain the same jet/runner speed ratio as in the reference point. The torque curves calculated by FLS and VOF methods are shown in Figure 16. The shape of the curves and the calculated efficiencies are similar with that corresponding to the reference point, while the only differences are the higher values of torque caused due to the increased kinetic energy of the jet. The agreement between FLS and Fluent results is again very good, with the same small systematic differences in the pattern of torque curve, and runner efficiency that differs only 0.3 percentage units (Figure 16).

5.4. FLS Performance for Modified Runner Design. Finally, a modified runner design was obtained by reducing the number of buckets from 22 to 18. In this case the angular distance between two consecutive buckets becomes 22.2% larger, while the amount of water jet that interacts with each bucket is also equally increased. This affects mainly the latest stage of jet-runner interaction, which becomes longer. As a result, the last part of outflow leaves the bucket lips at less optimum velocity, and in addition, more water exits from the cutout area. For this reason, the hydraulic efficiency of the runner becomes substantially lower, almost 2.5 percentage units as computed by Fluent (from 88.3% in Figure 12 to 85.9%).

This efficiency reduction is again reproduced well by the FLS method, as shown in Figure 17. As can be observed in this graph, the shape of the torque curves is also similar to the previous cases, but the deviation of FLS and Fluent values in the higher torque area (−20 to +5 degrees, Figure 17) becomes more pronounced.

These results support the previous discussion, according to which the irregularity of the VOF curve in this area was attributed to the Coanda effect and the impact of the back flow from the previous bucket. The peak of the torque curve is now displaced to higher angular positions of the bucket, at about −3°, compared to about −10° in the reference case (Figure 12). On the other hand, the FLS does not simulate this mechanism; hence its torque curve remains smooth and reaches maximum at about −13°, as in the reference case.

5.5. Models Performance and Comparison for Different Bucket Design. The Fluent-VOF and FLS models were finally applied to simulate the flow in a modified runner design obtained in [5]. The new runner is drastically different in terms of the bucket shape, including changes of the main dimensions, the scheme of the cut, and the exit angle, as shown in Figure 18. In addition, the number of buckets was 20 and their position was changed in terms of the radial distance from the center and their inclination.

The higher attainable efficiency of this new runner is confirmed by both Fluent and FLS computations, while its value obtained by the FLS exhibits again close agreement with the Fluent value, being only 0.5% higher (95% compared to 94.5%). However, the differences on the torque curves compared in Figure 19 are more pronounced than in the reference runner, especially in the beginning of the jet impact,

Table 1: Comparison of FLS and Fluent computational results.

Case description	Discharge (% of BEP)	Net head (m)	Runner speed (rpm)	Number of buckets	Eff. VOF (%)	Eff. FLS (%)
Reference point	100	100	1000	22	**88.3**	**88.5**
Low flow rate	50	100	1000	22	**91.2**	**91.3**
High flow rate	135	100	1000	22	**86.7**	**86.4**
High hydraulic head	100	156	1250	22	**88.2**	**88.5**
Modified runner	100	100	1000	18	**85.8**	**85.9**
Different bucket design	100	100	1000	20	**94.5**	**95.0**

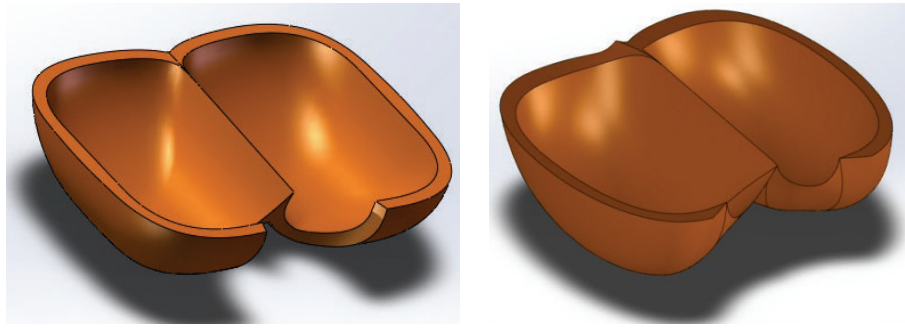

(a) (b)

Figure 18: Comparison of the reference bucket (a) and the modified bucket design (b).

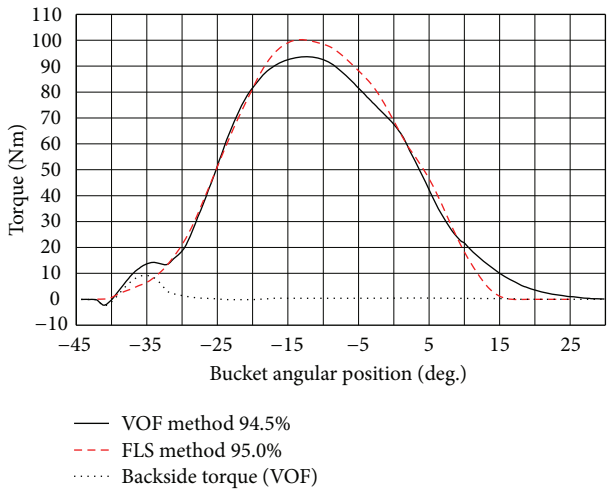

Figure 19: Comparison of VOF and FLS methods for a new modified runner design.

(at about −35 degrees), in the area of the maximum torque (−15 to −5 degrees), and to the end of the interaction (after +10 degrees).

These discrepancies were investigated by examining the characteristics of the flow in the new runner as computed by the VOF method, and it was found that the attachment of the flow at the backside of the new bucket is much more pronounced. A much larger portion of the jet flow remains attached there causing substantial torque due to the Coanda effect, as shown in Figure 19 (backside torque curve at −35 degrees). Afterwards, this diverged portion of water hits the leading bucket at an average angle of about −15 degrees, in agreement to available experimental results [19], but at reduced impact velocity, causing reduced peak torque values and delayed evacuation of the bucket. Although a different tuning of current FLS coefficients could mitigate the above deviations, the present results indicate that further development of the FLS model may be required in order to take into account the effects of this important flow mechanism. The structure and philosophy of the FLS method facilitate the introduction of such new relations.

5.6. Summary of Runner Efficiency Results. The results for the hydraulic efficiency of the runner obtained from the various test cases carried out in this study are concentrated in Table 1. As it can be seen, the agreement is in all cases very satisfactory, with maximum deviation of only 0.5 percentage units. Considering the much faster flow evaluation by the FLS algorithm, these results support its important advantage for being used for multiple evaluations, as required in parametric performance studies and numerical design optimization of Pelton turbines.

6. Conclusions

This work aims to validate the capability of a particulate numerical method, the Fast Lagrangian Simulation (FLS) algorithm, to reproduce in a reliable and accurate way the very complex flow created during the jet-runner interaction in Pelton turbines.

The method was compared with a more accurate Eulerian mesh-type VOF method, which has been validated in various previous works and proved to provide satisfactory results. The FLS model is tuned based on the numerical results at a reference operation point of a laboratory model turbine, and

then it is applied, together with the Eulerian method, to a number of different test cases, by modifying the flow rate, the hydraulic head and the number of buckets, and the bucket design of the runner.

In all these cases the hydraulic efficiency values obtained by the FLS method showed very good agreement with the Eulerian method results, while the predicted evolution of the free surface flow in the bucket, in terms of time variation of the developing torque, was also satisfactory.

The present results are very encouraging towards the implementation of the FLS tool to perform multiparametric and multiobjective design optimization studies in modern Pelton runners at very low computational cost. Further validation tests are needed using different runner and bucket shapes for a better and more general adjustment of the FLS coefficients, while further development in order to take into account the effect of other important mechanisms like the backside flow could enhance the accuracy of its results.

Finally, the presented results, along with the provided detailed geometric dimensions of the Pelton model runner, can constitute a benchmark set of data for the validation and evaluation of other numerical modelling tools and methods.

Conflict of Interests

The authors declare that there is no conflict of interests regarding the publication of this paper.

References

[1] A. Židonis and G. A. Aggidis, "State of the art in numerical modelling of Pelton turbines," *Renewable and Sustainable Energy Reviews*, vol. 45, pp. 135–144, 2015.

[2] L. F. Barstad, *CFD analysis of a Pelton turbine [M.S. thesis]*, Norwegian University of Science and Technology, Trondheim, Norway, 2012.

[3] A. Santolin, G. Cavazzini, G. Ardizzon, and G. Pavesi, "Numerical investigation of the interaction between jet and bucket in a Pelton turbine," *Proceedings of the Institution of Mechanical Engineers, Part A: Journal of Power and Energy*, vol. 223, no. 6, pp. 721–728, 2009.

[4] B. Zoppé, C. Pellone, T. Maitre, and P. Leroy, "Flow analysis inside a pelton turbine bucket," *Journal of Turbomachinery*, vol. 128, no. 3, pp. 500–511, 2006.

[5] A. Zidonis, A. Panagiotopoulos, G. A. Aggidis, J. S. Anagnostopoulos, and D. E. Papantonis, "Parametric optimisation of two Pelton turbine runner designs using CFD," *Journal of Hydrodynamics*, vol. 27, no. 3, pp. 840–847, 2015.

[6] J. R. Rygg, *CFD analysis of a Pelton turbine in openFOAM [M.S. thesis]*, Norwegian University of Science and Technology, Trondheim, Norway, 2013.

[7] J. C. Marongiu, E. Parkinson, S. Lais, F. Leboeuf, and J. Leduc, "Application of SPH-ALE method to pelton hydraulic turbines," in *Proceedings of the 5th International SPHERIC Workshop*, pp. 253–258, Manchester, UK, June 2010.

[8] J. S. Anagnostopoulos and D. E. Papantonis, "A fast Lagrangian simulation method for flow analysis and runner design in Pelton turbines," *Journal of Hydrodynamics B*, vol. 24, no. 6, pp. 930–941, 2012.

[9] J. S. Anagnostopoulos, P. K. Koukouvinis, F. G. Stamatelos, and D. E. Papantonis, "Optimal design and experimental validation of a Turgo model hydro turbine," in *Proceedings of the ASME 11th Biennial Conference on Engineering Systems Design and Analysis (ESDA '12)*, vol. 2, pp. 157–166, Nantes, France, July 2012.

[10] T. Staubli, A. Abgottspon, P. Weibel et al., "Jet quality and Pelton efficiency," in *Proceedings of the Hydro International Conference on Progress—Potential—Plans*, Lyon, France, 2009.

[11] R. Fiereder, S. Riemann, and R. Schilling, "Numerical and experimental investigation of the 3D free surface flow in a model Pelton turbine," *IOP Conference Series: Earth and Environmental Science*, vol. 12, no. 1, Article ID 012072, 2010.

[12] D. Benzon, A. Židonis, A. Panagiotopoulos, G. A. Aggidis, J. S. Anagnostopoulos, and D. E. Papantonis, "Numerical investigation of the spear valve configuration on the performance of Pelton and Turgo turbine injectors and runners," *Journal of Fluids Engineering*, vol. 137, no. 11, Article ID 111201, 2015.

[13] A. Rossetti, G. Pavesi, G. Ardizzon, and A. Santolin, "Numerical analyses of cavitating flow in a pelton turbine," *Journal of Fluids Engineering—Transactions of the ASME*, vol. 136, no. 8, Article ID 081304, 2014.

[14] J.-C. Marongiu, F. Leboeuf, J. Caro, and E. Parkinson, "Free surface flows simulations in Pelton turbines using an hybrid SPH-ALE method," *Journal of Hydraulic Research*, vol. 48, no. 1, pp. 40–49, 2010.

[15] P. Koukouvinis, *Development of a meshfree particle method for the simulation of steady and unsteady free surface flows: application and validation of the method on impulse hydraulic turbines [Ph.D. thesis]*, National Technical University of Athens, Athens, Greece, 2012.

[16] ANSYS, *ANSYS Fluent Theory Guide, Release 15*, ANSYS, Canonsburg, Pa, USA, 2013.

[17] ANSYS, *ANSYS Fluent User Guide, Release 15*, ANSYS, Canonsburg, Pa, USA, 2013.

[18] A. Perrig, *Hydrodynamics of the free surface flow in Pelton turbine buckets [Ph.D. thesis]*, Swiss Federal Institute of Technology, Lausanne, Switzerland, 2007.

[19] A. Perrig, F. Avellan, J.-L. Kueny, M. Farhat, and E. Parkinson, "Flow in a Pelton turbine bucket: numerical and experimental investigations," *Journal of Fluids Engineering*, vol. 128, no. 2, pp. 350–358, 2006.

[20] E. Parkinson, C. Neury, H. Garcin, G. Vullioud, and T. Weiss, "Unsteady analysis of a Pelton runner with flow and mechanical simulations," *International Journal on Hydropower and Dams*, vol. 13, no. 2, pp. 101–105, 2006.

[21] L. E. Klemetsen, *An experimental and numerical study of the free surface Pelton bucket flow [M.S. thesis]*, Norwegian University of Science and Technology, Trondheim, Norway, 2010.

[22] F. G. Stamatelos, J. S. Anagnostopoulos, and D. E. Papantonis, "Performance measurements on a Pelton turbine model," *Proceedings of the Institution of Mechanical Engineers Part A: Journal of Power and Energy*, vol. 225, no. 3, pp. 351–362, 2011.

[23] International Electrotechnical Commission, "Hydraulic turbines, storage pumps and pump-turbines—model acceptance tests," Standard IEC 60193, International Electrotechnical Commission, 1999.

[24] M. Nechleba, *Hydraulic Turbines: Their Design and Equipment*, Artia, Prague, Czech Republic, 1957.

[25] J. Thake, *The Micro-Hydro Pelton Turbine Manual: Design, Manufacture and Installation for Small-Scale Hydro-Power*, ITDG publishing, London, UK, 2000.